

# Two-lifetime model for the cuprates revisited

Lucia Gelenekyová, František Herman, Hana Havranová, and Richard Hlubina

Department of Experimental Physics, Comenius University, Mlynská Dolina F2, 842 48 Bratislava, Slovakia

(Dated: February 3, 2026)

Several models of the strange-metal state of the cuprate superconductors postulate the existence of strong inelastic forward scattering of the electrons, but direct evidence of such scattering is missing. Here we show that angle-resolved photoemission spectroscopy (ARPES) provides a unique tool which can address this issue. We propose a two-lifetime phenomenological model of the superconducting state of the cuprates and we show that it explains several salient low-energy features of the measured ARPES spectra. The model enables discrimination between forward- and large-angle scattering and, in addition, gives access to the magnitude of the gap function away from the Fermi surface.

After nearly four decades of intensive studies, the cause of the anomalies observed in the non-superconducting state of the cuprate superconductors remains mysterious [1, 2]. Strong forward scattering is often considered to be responsible for the observed anomalous behavior [3–8]. But, by definition, the effect of such scattering on transport is strongly reduced. Does it mean that forward scattering is not directly observable? In this paper we show that this is not the case, since angle-resolved photoemission spectroscopy (ARPES) of the superconducting state provides a unique tool for distinguishing between forward and large-angle scattering in the cuprates.

To illustrate the general idea in a controlled way, we consider the case of low temperatures  $T$ , when impurity scattering should dominate. In an anisotropic singlet superconductor, generic impurity scattering is pair-breaking [9]. However, the special case of forward- and  $2k_F$ -scattering is pair-conserving [9] and obeys Anderson's theorem [10]. One can argue that a large part of impurity scattering in the cuprates is of forward-scattering type [11]. The reason is simple: the  $\text{CuO}_2$  planes are held together by strong covalent bonds, and therefore they are well protected against defects. On the other hand, outside these planes, disorder is generically present. Simple estimates lead then to the conclusion that out-of-plane disorder has to generate forward scattering [11].

Thus, in order to phenomenologically describe the low- $T$  superconducting state of the cuprates, the BCS theory has to be generalized at the very least by including both types of impurity scattering, pair-conserving (due to forward scattering) and pair-breaking (due to large-angle scattering). In case of isotropic  $s$ -wave superconductors, a convenient two-lifetime generalization of the BCS theory has been worked out recently [12]. The resulting electronic Green's function, leading to the Dynes formula [13] for the density of states, is given by an explicit expression with several favourable properties [14]: it is analytic in the upper half-plane, it has correct large-energy asymptotics, its spectral function is positive definite, and it does not break the particle-hole symmetry. Within this theory a superconductor is characterized by three energy scales: superconducting gap  $\Delta$ , pair-breaking scattering rate  $\Gamma$ , and pair-conserving scattering rate  $\Gamma_s$ . The parameters  $\Delta$  and  $\Gamma$  enter the Dynes formula [13].

In order to describe anisotropic superconductors such

as the cuprates, here we make use of what we will call momentum-resolved Dynes phenomenology (MRDP). Within MRDP, we postulate that for every momentum  $\mathbf{k}$ , the energy dependence of the electron Green's function is described by the theory of Dynes superconductors [12, 14] with “local” values of the parameters  $\Delta(\mathbf{k})$ ,  $\Gamma_s(\mathbf{k})$ , and  $\Gamma(\mathbf{k})$ . We will demonstrate that MRDP is a suitable framework for description of the available ARPES data for the cuprates, thereby giving us a unique tool for a direct measurement of the magnitude of forward and large-angle scatterings, respectively.

The idea that a two-lifetime phenomenology is necessary in order to describe the superconducting state of the cuprates is not new. In fact, in [15] the authors introduced the concept of the tomographic density of states (TDoS) and showed that TDoS can be described by the Dynes formula. The Dynes parameter  $\Gamma$  turned out to be much smaller than the quasiparticle width. Building on this observation in [16] the authors argued, by means of an analysis of spectral functions at  $k = k_F$ , that two lifetimes are necessary to fit the data. However, the analysis in [16] was based on an unphysical formula for the Green's function proposed in [17]. Moreover, the interpretation of the two lifetimes was unclear.

Here we present a substantially improved continuation of the program initiated in [15, 16]. We make use of MRDP which enables a clear interpretation of the physical meaning of the two lifetimes. Moreover, we demonstrate that the necessity of introducing two lifetimes is much more evident in different aspects of ARPES than in the  $k = k_F$  data.

Let us start by noting that the MRDP Green's function of an electron with momentum  $\mathbf{k}$  and energy  $\omega$ , derived in Refs. [12, 14], can be rewritten in a BCS-like form:

$$G(\mathbf{k}, \omega) = \frac{U^2(\omega)}{\Omega + i\Gamma_s - \varepsilon_{\mathbf{k}}} + \frac{V^2(\omega)}{\Omega + i\Gamma_s + \varepsilon_{\mathbf{k}}}. \quad (1)$$

For the sake of brevity, if no confusion arises, we do not indicate the  $\mathbf{k}$ -dependence of  $\Delta$ ,  $\Gamma_s$ , and  $\Gamma$ . In Eq. (1) we have introduced a complex  $\omega$ -dependent energy scale  $\Omega(\omega) = \sqrt{(\omega + i\Gamma)^2 - \Delta^2} = \Omega_1 + i\Omega_2$ , where the square root is taken so that  $\Omega_1(\omega)$  is an odd function of  $\omega$ , while  $\Omega_2(\omega)$  is even and positive, see [18]. We have also intro-

duced the following  $\omega$ -dependent weight factors:

$$U^2(\omega) = \frac{\omega + i\Gamma + \Omega}{2\Omega}, \quad V^2(\omega) = \frac{\omega + i\Gamma - \Omega}{2\Omega}.$$

The electron spectral function is given by the usual expression  $A(\mathbf{k}, \omega) = -\text{Im}[G(\mathbf{k}, \omega)]/\pi$ . When the pair-conserving scattering rate  $\Gamma_s$  vanishes, it simplifies to

$$A(\mathbf{k}, \omega) = u_{\mathbf{k}}^2 \delta_{\Gamma}(\omega - E_{\mathbf{k}}) + v_{\mathbf{k}}^2 \delta_{\Gamma}(\omega + E_{\mathbf{k}}), \quad (2)$$

where the symbol  $\delta_{\Gamma}(x)$  stands for a Lorentzian with width  $\Gamma$ ,  $\delta_{\Gamma}(x) \equiv \pi^{-1}\Gamma/(x^2 + \Gamma^2)$ . This means that the spectral function consists of just two peaks at energies  $\pm E_{\mathbf{k}}$  where  $E_{\mathbf{k}} = \sqrt{\varepsilon_{\mathbf{k}}^2 + \Delta^2}$  is the BCS quasiparticle energy, with the BCS weight factors  $u_{\mathbf{k}}^2 = (E_{\mathbf{k}} + \varepsilon_{\mathbf{k}})/(2E_{\mathbf{k}})$  and  $v_{\mathbf{k}}^2 = (E_{\mathbf{k}} - \varepsilon_{\mathbf{k}})/(2E_{\mathbf{k}})$ . In the limit  $\Gamma \rightarrow 0$ , Eq. (2) further simplifies to the standard BCS result.

Conversely, if the pair-conserving scattering rate  $\Gamma_s$  is finite but  $\Gamma = 0$ , the spectral function is strictly zero inside the gap, i.e. for  $|\omega| < \Delta$ , while for  $|\omega| > \Delta$  we find

$$A(\mathbf{k}, \omega) = U^2(\omega) \delta_{\Gamma_s}(\Omega_1 - \varepsilon_{\mathbf{k}}) + V^2(\omega) \delta_{\Gamma_s}(\Omega_1 + \varepsilon_{\mathbf{k}}). \quad (3)$$

Since in this case  $\Omega_1 = \text{sgn}(\omega) \sqrt{\omega^2 - \Delta^2}$ , the Lorentzians again exhibit peaks at  $\omega = \pm E_{\mathbf{k}}$ . The spectral function contains also two other peaks at  $\omega = \pm \Delta$ , where the prefactors  $U^2(\omega)$  and  $V^2(\omega)$  exhibit square-root singularities.

In the general case when both  $\Gamma$  and  $\Gamma_s$  are finite, for  $\varepsilon_{\mathbf{k}} \neq 0$  the spectral function again exhibits a four-peak structure with the peaks located at energies  $\pm E_{\mathbf{k}}$  and  $\pm \Delta$ , but the singularities at  $\pm \Delta$  predicted by Eq. (3) are smeared by the finite value of  $\Gamma$ , see Ref. [14] for details.

We stress that one can discriminate between  $\Gamma_s$  and  $\Gamma$  only in the superconducting state. When  $\Delta = 0$ ,  $A(\mathbf{k}, \omega)$  is a Lorentzian with width  $\Gamma_{\text{tot}} = \Gamma_s + \Gamma$ , thus only the total scattering rate  $\Gamma_{\text{tot}}$  can be extracted from  $A(\mathbf{k}, \omega)$ .

In what follows MRDP will be applied to several aspects of the measured low-energy ARPES spectra in the cuprates [15, 16, 19–25]. We consider the simplest normal-state electron dispersion capturing the gross features of the cuprates,  $\varepsilon_{\mathbf{k}} = -2t(\cos k_x a + \cos k_y a) + 4t' \cos k_x a \cos k_y a - \mu$ . Here  $a$  is the lattice constant,  $t = 0.335$  eV and  $t' = 0.125$  eV are hopping amplitudes, and  $\mu = -0.48$  eV is the chemical potential. The superconducting state is described by the  $d$ -wave gap  $\Delta_{\mathbf{k}} = \Delta_d(\cos k_x a - \cos k_y a)/2$ .

TDoS can be found by integrating the spectral functions along a fixed "tomographic" cut perpendicular to the Fermi surface,  $N(\omega, \theta) = \int dk A(k, \theta, \omega)$  [15]. Here, we parametrize  $\mathbf{k}$  by  $(k, \theta)$ , where the angle  $\theta$  defines the tomographic cut, see Fig. 1e, and  $k$  measures the position along the cut. Starting with Eq. (1) and neglecting the (presumably) weak dependence of  $\Delta(k, \theta)$ ,  $\Gamma(k, \theta)$ , and  $\Gamma_s(k, \theta)$  on  $k$ , we find that  $N(\omega, \theta)$  is within MRDP proportional to the Dynes formula  $n(\omega, \theta) = \text{Re}[(\omega + i\Gamma)/\Omega(\omega)]$ , in agreement with the experimental results [15]. Note that TDoS does not depend on the value of  $\Gamma_s(\theta)$ , but only on the local values of  $\Gamma(\theta)$  and  $\Delta(\theta)$ . Using the recent low-temperature data for

overdoped Bi2212 presented in Ref. [19] we find that  $\Gamma(\theta)$  lies in the range of 2.5 – 4.5 meV with a maximum roughly in the middle between the nodal and antinodal directions. This is in reasonable agreement with the roughly isotropic pair-breaking scattering rate  $\Gamma \sim \Delta_d/10 \approx 3$  meV observed in the near-nodal regime of optimally doped Bi2212 in Ref. [15]. Overdoped samples of Bi2212 also exhibit  $\Gamma \sim \Delta_d/10 \approx 3$  meV in the near-nodal region at low temperatures [20].

Next we study the spectral function  $A(\mathbf{k}, \omega)$  for fixed  $\omega$  as a function of momentum  $\mathbf{k}$  in the 2D Brillouin zone, to be called the momentum map. In overdoped but still superconducting Bi2201 it was recently found that the momentum map at the chemical potential, i.e. for  $\omega = 0$ , resembles that of a normal metal [21]. This result might look anomalous, but it can be easily interpreted by MRDP. In fact, for  $\omega = 0$  Eq. (1) implies that

$$A(\mathbf{k}, 0) = w(\theta) \delta_{\Gamma_{\text{eff}}}(\varepsilon_{\mathbf{k}}). \quad (4)$$

Thus, the  $\omega = 0$  momentum map consists of Lorentzians along tomographic cuts with maxima at the normal-state Fermi surface  $\varepsilon_{\mathbf{k}} = 0$ , angle-dependent widths  $\Gamma_{\text{eff}}(\theta) = \Gamma_s + \sqrt{\Gamma^2 + \Delta^2}$ , and weights  $w(\theta) = \Gamma/\sqrt{\Gamma^2 + \Delta^2}$ . Momentum maps calculated using Eq. (4) in the Brillouin zone of a model cuprate superconductor are shown in Fig. 1. For  $\Gamma \ll \Delta_d$  (Fig. 1a), the spectral function is finite only in the vicinity of the nodal point, as expected. However, for a pair-breaking rate  $\Gamma$  comparable to  $\Delta_d$  (Fig. 1b), the momentum map resembles the experimental results of [21].

The momentum map at energy  $\omega < 0$  of a BCS superconductor with vanishing scattering rates  $\Gamma$  and  $\Gamma_s$  is finite only at those  $\mathbf{k}$ -points where  $E_{\mathbf{k}} = -\omega$ , see Fig. 1e. Finite values of both,  $\Gamma$  and  $\Gamma_s$ , contribute to the broadening of these so-called bananas. However,  $\Gamma_s$  produces an additional effect: it generates a finite signal along the "gap arcs" where  $|\Delta_{\mathbf{k}}| = -\omega$ , also shown in Fig. 1e. As a result, the spectral function in the ends of the bananas (i.e., at angle  $\theta_0$ ) is enhanced with respect to their interior, as predicted theoretically long ago by Markiewicz [26]. More quantitatively, the maximal spectral function (as a function of  $k$ ) in the nodal direction is  $A_{\text{norm}} = 1/(\pi\Gamma_{\text{tot}})$ . We estimate  $\theta_0$  as the angle where  $\omega^2 = \Delta(\theta_0)^2 + \Gamma(\theta_0)^2$  holds. The ratio between  $A_{\text{norm}}$  and the spectral function in the bright spots at the end of the bananas,  $A_{\text{bright}} = A(k_F, \theta_0)$ , strongly depends on the value of  $\Gamma_s$ . For  $\Gamma_s = 0$  we find  $A_{\text{bright}}/A_{\text{norm}} = 1/2$ , whereas for  $\Gamma_s \gg \Delta \gg \Gamma$ , we estimate  $A_{\text{bright}}/A_{\text{norm}} \approx \sqrt{\Delta/(4\Gamma)} \gg 1$ . This effect is demonstrated explicitly in Figs. 1c,d, where we compare momentum maps for  $\Gamma_s = 0$  and  $\Gamma_s \neq 0$ . Remarkably, the very recently found bright spots at the ends of the bananas in momentum maps at finite energy  $\omega$  in moderately underdoped Bi2212 [22] strongly support our MRDP modeling with finite values of  $\Gamma_s$ . We emphasize that all maps in Fig. 1 are completely determined by the low-energy properties of the spectral functions. For

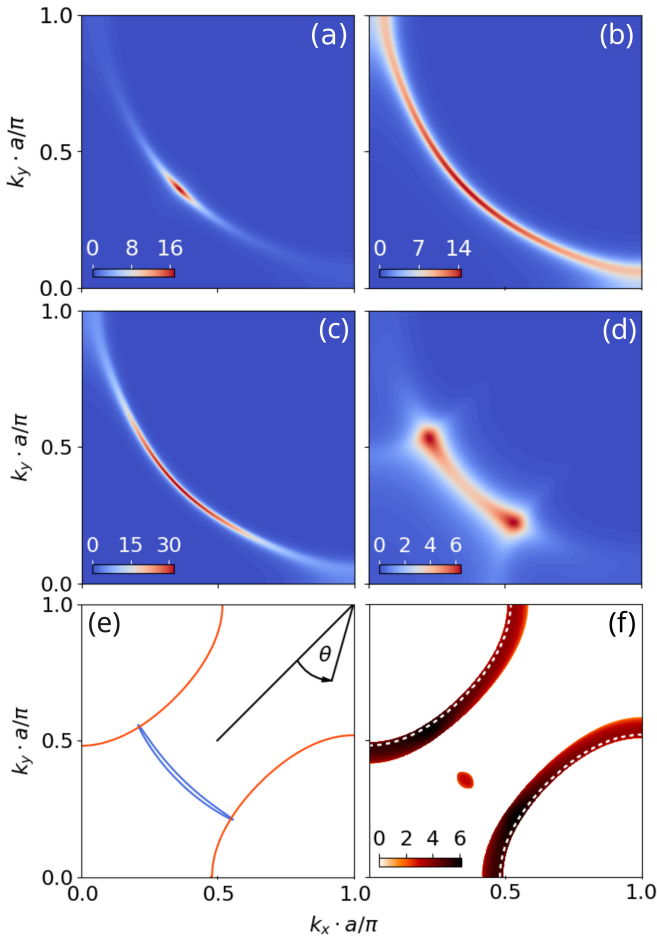


FIG. 1. (a-d): Momentum maps of  $A(\mathbf{k}, \omega)$  predicted by MRDP for model superconductors with momentum-independent scattering rates  $\Gamma$  and  $\Gamma_s$ . (a,b) shows data at the chemical potential  $\omega = 0$  for  $\Gamma_s = 16$  meV. (a):  $\Delta_d = 30$  meV and  $\Gamma = 3$  meV. (b):  $\Delta_d = 6$  meV and  $\Gamma = 6$  meV. (c,d) shows data at finite energy  $\omega = -14$  meV for  $\Delta_d = 30$  meV. (c):  $\Gamma = 10$  meV and  $\Gamma_s = 0$ . (d):  $\Gamma = 2$  meV and  $\Gamma_s = 80$  meV. (e): Definition of the angle  $\theta$ . Also shown is the banana-shaped line where  $E_{\mathbf{k}} = -\omega$  (blue line) and the gap arcs where  $|\Delta_{\mathbf{k}}| = -\omega$  (red lines) for the same parameters as in (c,d). (f): Momentum map of the logarithm of the second derivative of the data in (d) with respect to energy,  $\log[-A''(\mathbf{k}, \omega)]$ . Only points where  $A''(\mathbf{k}, \omega) < 0$  are shown. White dashed lines show the gap arcs.

an analysis of the so-called joint density of states also measured in [22], see [18].

Much more common in the literature than the momentum maps are 2D plots of the spectral function  $A(k, \theta, \omega)$  at fixed angle  $\theta = \text{const}$ , to be called tomographic maps in what follows. For recent examples of experimental tomographic cuts for the cuprates, see Refs. [23–25]. A commonly observed feature of tomographic cuts, which does not seem to have attracted attention so far, is that the maximal spectral weight at a fixed energy  $\omega$ ,  $A_{\max}(\omega) = \max_k A(k, \omega)$ , increases as  $|\omega|$  moves towards the energy gap  $|\omega| \approx \Delta$ . Note that

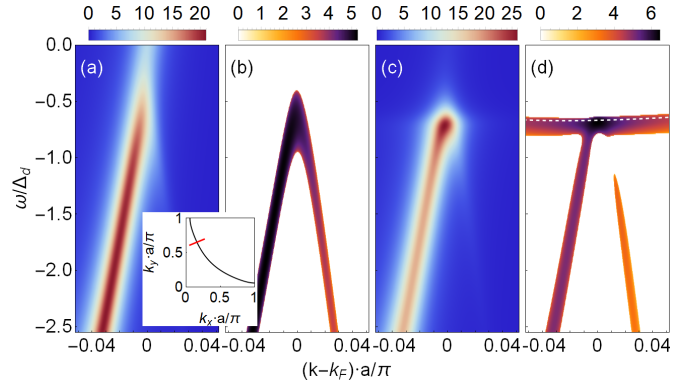


FIG. 2. (a,c): Tomographic maps of  $A(\mathbf{k}, \omega)$  predicted by MRDP along the path indicated in the inset for a superconductor with  $\Delta_d = 30$  meV. (b,d): Logarithm of the second derivatives with respect to energy  $\log[-A''(\mathbf{k}, \omega)]$  of the same data. Only points where  $A''(\mathbf{k}, \omega) < 0$  are shown. (a,b):  $\Gamma = 15$  meV and  $\Gamma_s = 0$  meV. (c,d):  $\Gamma = 3$  meV and  $\Gamma_s = 15$  meV. White dashed line in (d): the function  $\omega = -\Delta_{\mathbf{k}}$  along the tomographic cut.

for large  $|\omega|$ , within MRDP  $A_{\max}(\omega) = A_{\text{norm}}$ . On the other hand, for energy  $\omega_* = \sqrt{\Delta^2 + \Gamma^2}$  close to the gap  $A_{\max}(-\omega_*) \approx A(k_F, |\omega_*|) = A_{\text{bright}}$ . Therefore, the modulation of the spectral function  $A$  along the BCS line  $\omega = -E_{\mathbf{k}}$  in the tomographic cut exhibits the same behavior as the modulation of  $A$  along the banana in the momentum map: in both maps, one compares the magnitude of  $A$  at  $k = k_F$  with  $A$  for momenta far away from the Fermi surface. As a result, a finite  $\Gamma_s$  is required in order that MRDP resembles the experimental tomographic maps. This is explicitly demonstrated in the numerically obtained tomographic maps presented in Fig. 2. It is pleasing to note that, also on the experimental side, bright spots are consistently found both in momentum maps [22], as well as in tomographic maps [23–25].

The MRDP parameters  $\Delta$ ,  $\Gamma_s$ , and  $\Gamma$  can be determined most straightforwardly by fitting the ARPES spectra at the Fermi surface  $k = k_F$ , since these do not depend on the energy dispersion  $\varepsilon_{\mathbf{k}}$ . In Fig. 3 we plot the MRDP parameters obtained by fitting the data from Ref. [16] for optimally doped Bi2212 at  $\theta = 24^\circ$ . For an explicit formula for the spectral function at  $k = k_F$  and details of the fitting procedure, see [18]. As expected, at low temperatures both scattering rates are dominated by elastic processes, since they are  $T$ -independent. We find that  $\Gamma_s \gg \Gamma$ , in agreement with the picture proposed in Ref. [11]. Inelastic scattering starts to appreciably influence  $\Gamma_s$  and  $\Gamma$  at  $\approx 50$  K.

In Fig. 4 we plot the angular dependence of the low- $T$  MRDP parameters for data from Ref. [16]. The extracted pair-breaking rate  $\Gamma$  is weakly angle-dependent, in agreement with analysis of the TDoS data [15, 19, 20]. We identify  $\Gamma$  with the isotropic scattering rate  $\Gamma_{\text{iso}}$  found by magnetotransport [27] and an earlier normal-state ARPES study [28]. In fact, close to  $T_c$ , the magnitude

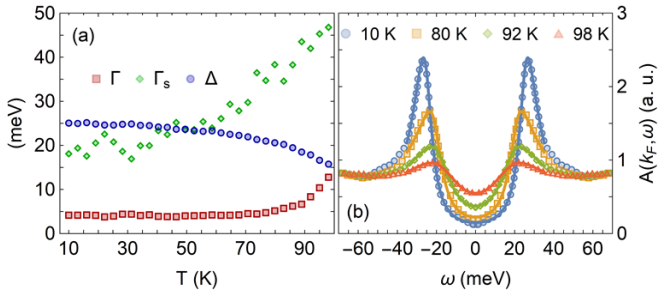


FIG. 3. (a): Temperature dependence of the MRPD parameters obtained by fitting the spectral functions at  $k = k_F$  and  $\theta = 24^\circ$  in optimally doped Bi2212, taken from Ref. [16]. In agreement with Refs. [15, 16, 19, 24], the gap and the scattering rates are continuous across the critical temperature  $T_c = 92$  K. (b): Spectral functions (symbols) and their MRPD fits (lines) for selected temperatures.

of  $\Gamma$  roughly agrees with  $\Gamma_{\text{iso}} \approx 0.6k_B T$  found in [27] and with  $\Gamma_{\text{iso}} \approx 0.7\omega$  from [28], see Fig. 3. Similarly, we identify  $\Gamma_s$  with the anisotropic scattering rate  $\Gamma_{\text{aniso}}$  found in Refs. [27, 28], since both exhibit a similar dependence on the angle  $\theta$ . Figure 3 shows that, close to  $T_c$ , our extracted  $\Gamma_s$  is roughly consistent with normal-state ARPES [28]. At the same time, it is much larger than  $\Gamma_{\text{aniso}}$  found by magnetotransport [27], providing an independent support of its forward-scattering origin. Surprisingly, we find that  $\Gamma_s$  is  $T$ -dependent at  $T < T_c$ : this is different from the normal-state result that  $\Gamma_{\text{aniso}}$  is independent of temperature [27] and energy [28].

Having presented a set of arguments strongly supporting the applicability of MRPD to the cuprates, in the rest of this paper we propose that ARPES offers, in addition, a unique possibility to measure the so-far unexplored momentum dependence of the gap function  $\Delta_{\mathbf{k}}$  also away from the Fermi surface. Such information, if available, would provide an additional constraint on the acceptable pairing mechanism in the cuprates. To this end, let us reconsider Fig. 1d, where we plot the momentum map of  $A(\mathbf{k}, \omega)$  for large forward scattering rate  $\Gamma_s$  and small pair-breaking rate  $\Gamma$ . Note that the gap arcs where  $|\Delta_{\mathbf{k}}| = -\omega$  start to be visible in such a map, thereby providing direct access to the gap function. Since  $A(\mathbf{k}, -\Delta_{\mathbf{k}})$  grows with  $\Gamma_s$  and decreases with  $\Gamma$ , in order to measure  $\Delta_{\mathbf{k}}$ , one will need to study samples with large disorder away from the  $\text{CuO}_2$  planes, keeping the in-plane disorder as small as possible.

Surprisingly, the  $|\Delta_{\mathbf{k}}| = -\omega$  part of the electron spectral function might have already been observed. In fact, the authors of Ref. [25] have calculated the second derivative of the measured spectral function with respect to energy,  $A''(\mathbf{k}, \omega)$ , in order to emphasize the local maxima of the spectral function  $A(\mathbf{k}, \omega)$ . Besides other features, they have found large values of  $-A''(\mathbf{k}, \omega)$  at  $\omega \approx -|\Delta_{\mathbf{k}}|$ . Our Fig. 2 shows that, within MRPD, taking the second derivative does strongly emphasize the  $\omega = -|\Delta_{\mathbf{k}}|$  branch of the tomographic map of the spectral function

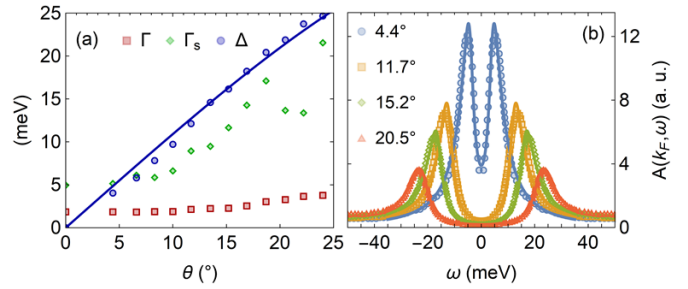


FIG. 4. (a): Angular dependence of the MRPD parameters for spectral functions at  $k = k_F$  and  $T = 10$  K in optimally doped Bi2212, taken from Ref. [16]. The line is a fit to  $\Delta_{\mathbf{k}} = \Delta_d(\cos k_y a - \cos k_x a)/2$  with  $\Delta_d = 34.8$  meV. For  $\theta = 0^\circ$  we can determine only  $\Gamma_{\text{tot}} = \Gamma_s + \Gamma = 7$  meV; individual values of  $\Gamma$  and  $\Gamma_s$  are assigned by hand. (b): Spectral functions (symbols) and their MRPD fits (lines) for selected angles.

(for theoretical justification, see [18]). Therefore, we believe that the signal found in [25] should be interpreted as a measurement of the function  $\Delta_{\mathbf{k}}$  along the tomographic cut. In Fig. 1f we show that plotting the momentum map of the second energy derivative  $A''(\mathbf{k}, \omega)$  should improve the visibility of the gap arc  $|\Delta_{\mathbf{k}}| = -\omega$  also in momentum maps. Alternatively, one might study maps of the ratio between superconducting and normal spectral functions.

Before concluding, let us point out that, within the standard Eliashberg theory, one introduces two self-energies,  $\Sigma(\omega)$  and  $\Phi(\omega)$ , both of which depend on frequency  $\omega$  and the angle  $\theta$ . In terms of these functions, the full Nambu-Gorkov  $2 \times 2$  Green's function reads

$$\hat{G}(\mathbf{k}, \omega) = \frac{(\omega - \Sigma)\tau_0 + \Phi\tau_1 + \varepsilon_{\mathbf{k}}\tau_3}{(\omega - \Sigma)^2 - \Phi^2 - \varepsilon_{\mathbf{k}}^2}, \quad (5)$$

where  $\tau_i$  are the Pauli matrices. The Green's function Eq. (1) is its 11 component,  $G(\mathbf{k}, \omega) \equiv \hat{G}_{11}(\mathbf{k}, \omega)$ . In the ARPES literature, the Green's function is often described by  $G(\mathbf{k}, \omega) = [\omega - \varepsilon_{\mathbf{k}} - \mathcal{S}(\mathbf{k}, \omega)]^{-1}$ , where  $\mathcal{S}(\mathbf{k}, \omega)$  is what we will call the "photoemission self-energy". The Eliashberg theory implies that

$$\mathcal{S}(\mathbf{k}, \omega) = \Sigma + \frac{\Phi^2}{\omega - \Sigma + \varepsilon_{\mathbf{k}}}. \quad (6)$$

In the widely used Norman's formula (NF) for the photoemission self-energy [17] one assumes that  $\Phi = \Delta$ , and replaces  $\Sigma$  by  $-i\Gamma_1$  in the first term of Eq. (6), and by  $-i\Gamma_0$  in the denominator of the second term. Thus, the NF Green's function is not compatible with the Eliashberg theory. In [14] we have shown that, for  $\varepsilon_{\mathbf{k}} \neq 0$ , NF is inconsistent with the exact sum rules for the particle number, because the electronlike and holelike branches exhibit different scattering rates. Here we make an additional observation that, even if we take NF as a purely phenomenological formula for  $\omega < 0$ , it does not correctly describe the observed low-temperature data. The reason is that, in the experimentally relevant range of parameters  $\Gamma_0 \ll \Gamma_1 \lesssim \Delta$  [16], NF does not generate

the experimentally observed bright spots at  $k = k_F$ . On the other hand, MRDP does reproduce the measured self energies, see [18].

In conclusion, we have shown that ARPES spectroscopy of the superconducting state offers a unique possibility to distinguish between forward- and large-angle scattering processes in the cuprates. Although we have considered only strictly elastic scattering, we hope that our conclusions apply at least qualitatively also to inelastic scattering by low-lying modes. A detailed study of the angle- and temperature-dependence of the forward- and large-angle scattering rates  $\Gamma_s$  and  $\Gamma$ , respectively, might therefore provide hitherto inaccessible information on the dynamics of the electrons in the cuprates [29]. We have

also suggested a novel method for measuring the superconducting gap  $\Delta_{\mathbf{k}}$  away from the Fermi surface. The method should work best at low  $T$ , when pair-breaking scattering is minimized. Large forward scattering is also needed, and this can be realized by selectively increasing disorder outside the  $\text{CuO}_2$  planes.

*Acknowledgements.* This work was supported by the Slovak Research and Development Agency under Contract No. APVV-23-0515 and by the European Union's Horizon 2020 research and innovation programme under the Marie Skłodowska-Curie Grant Agreement No. 945478.

L.G. and F.H. contributed equally to this work.

---

[1] B. Keimer, S.A. Kivelson, M.R. Norman, S. Uchida, and J. Zaanen, *Nature* **518**, 179 (2015).

[2] C.M. Varma, *Rev. Mod. Phys.* **92**, 031001 (2020).

[3] P.W. Anderson, *The theory of high temperature superconductivity* (Princeton University Press, NY, 1996).

[4] P.A. Lee and N. Nagaosa, *Phys. Rev. B* **46**, 5621 (1992).

[5] C.M. Varma, *Phys. Rev. B* **73**, 155113 (2006).

[6] X. Wang and E. Berg, *Phys. Rev. B* **99**, 235136 (2019).

[7] P.W. Phillips, L. Yeo, and E.W. Huang, *Nature Physics* **16**, 1175 (2020).

[8] S. Kukreja, D.M. Willerton, and Sung-Sik Lee, arXiv:2601.21047.

[9] A.J. Millis, S. Sachdev, and C.M. Varma, *Phys. Rev. B* **37**, 4975 (1988).

[10] P.W. Anderson, *J. Phys. Chem. Solids* **11**, 26 (1959).

[11] E. Abrahams and C. Varma, *Proc. Natl. Acad. Sci. USA* **97**, 5714 (2000).

[12] F. Herman and R. Hlubina, *Phys. Rev. B* **94**, 144508 (2016).

[13] R.C. Dynes, V. Narayanamurti, and J.P. Garno, *Phys. Rev. Lett.* **41**, 1509 (1978).

[14] F. Herman and R. Hlubina, *Phys. Rev. B* **95**, 094514 (2017).

[15] T. J. Reber, N. C. Plumb, Z. Sun, Y. Cao, Q. Wang, K. McElroy, H. Iwasawa, M. Arita, J. S. Wen, Z. J. Xu, G. Gu, Y. Yoshida, H. Eisaki, Y. Aiura, and D. S. Dessau, *Nature Physics* **8**, 606-610 (2012).

[16] T. Kondo, W. Malaeb, Y. Ishida, T. Sasagawa, H. Sakamoto, T. Takeuchi, T. Tohyama, and S. Shin, *Nat. Commun.* **6**, 7699 (2015).

[17] M.R. Norman, M. Randeria, H. Ding, and J.C. Campuzano, *Phys. Rev. B* **57**, R11093(R) (1998).

[18] See Supplemental Material at [http://link.aps.org/...](http://link.aps.org/) for the definition of  $\Omega_{1,2}(\omega)$ , results for the spectral functions in various limiting cases, technical details on the fits to the experimental data at  $k = k_F$ , and prediction of MRDP for the Eliashberg self-energies and joint density of states, which include Ref. [30].

[19] S.-D. Chen, M. Hashimoto, Y. He, D. Song, J.-F. He, Y.-F. Li, S. Ishida, H. Eisaki, J. Zaanen, T. P. Devreux, D.-H. Lee, D.-H. Lu, and Z.-X. Shen, *Nature* **601**, 562–567 (2022).

[20] T. J. Reber, S. Parham, N. C. Plumb, Y. Cao, H. Li, Z. Sun, Q. Wang, H. Iwasawa, M. Arita, J. S. Wen, Z. J. Xu, G.D. Gu, Y. Yoshida, H. Eisaki, G.B. Arnold, and D. S. Dessau, arXiv: 1508.06252 (2015).

[21] S. Ye, M. Xu, H. Yan, Z.-X. Li, C. Zou, X. Li, Y. Chen, X. Zhou, D.-H. Lee and Y. Wang, *Nat. Commun.* **15**, 4939 (2024).

[22] N.K. Shah, J. Zhao, and U. Chatterjee, arXiv:2509.12568.

[23] J.M. Bok, J.J. Bae, H.-Y. Choi, C.M. Varma, W. Zhang, J. He, Y. Zhang, L. Yu, and X.J. Zhou, *Sci. Adv.* **2**, e1501329 (2016).

[24] H. Li, X. Zhou, S. Parham, T.J. Reber, H. Berger, G.B. Arnold, and D.S. Dessau, *Nat. Commun.* **9**, 26 (2018).

[25] H. Yan, J.M. Bok, J. He, W. Zhang, Q. Gao, X. Luo, Y. Cai, Y. Peng, J. Meng, C. Li, H. Chen, C. Song, C. Yin, T. Miao, Y. Chen, G. Gu, C. Lin, F. Zhang, F. Yang, S. Zhang, Q. Peng, G. Liu, L. Zhao, H.-Y Choi, Z. Xu, and X. J. Zhou, *PNAS* **120**, e2219491120 (2023).

[26] R.S. Markiewicz, *Phys. Rev. B* **69**, 214517 (2004).

[27] G. Grissonnanche, Y. Fang, A. Legros, S. Verret, F. Laliberté, C. Collignon, J. Zhou, D. Graf, P.A. Goddard, L. Taillefer, and B.J. Ramshaw, *Nature* **595**, 667 (2021).

[28] A. Kaminski, H. M. Fretwell, M. R. Norman, M. Randeria, S. Rosenkranz, U. Chatterjee, J. C. Campuzano, J. Mesot, T. Sato, T. Takahashi, T. Terashima, M. Takano, K. Kadowaki, Z.Z. Li, and H. Raffy, *Phys. Rev. B* **71**, 014517 (2005).

[29] More precisely speaking, the inelastic part of  $\Gamma_s(T)$  in a singlet superconductor is a measure of the sum of forward and  $2k_F$  scattering.

[30] The octet model was introduced to interpret the quasi-particle interference observed by scanning tunneling spectroscopy of the cuprates, see K. McElroy, R. W. Simmonds, J. E. Hoffmann, D.-H. Lee, J. Orenstein, H. Eisaki, S. Uchida, and J. C. Davis, *Nature* **422**, 592 (2003).

## Supplemental Material: Two-lifetime model for the cuprates revisited

Lucia Gelenekyová, František Herman, Hana Havranová, and Richard Hlubina

*Department of Experimental Physics, Comenius University, Mlynská Dolina F2, 842 48 Bratislava, Slovakia*

(Dated: February 2, 2026)

**Sign convention for  $\Omega(\omega)$ .** The real and imaginary parts of  $\Omega(\omega)$  are explicitly given by

$$\Omega_1 = \text{sgn}(\omega) \{[(z^2 + 4\omega^2\Gamma^2)^{1/2} + z]/2\}^{1/2}, \quad \Omega_2 = \{[(z^2 + 4\omega^2\Gamma^2)^{1/2} - z]/2\}^{1/2}, \quad (\text{S1})$$

where  $z = \omega^2 - \omega_*^2$ .

**Analysis of the spectral function at the Fermi surface.** At the Fermi surface, the spectral function is given by

$$A(k_F, \omega) = \frac{1}{\pi} \frac{\Gamma(\omega^2 + \omega_*^2) + \Gamma_s(\omega\Omega_1 + \Gamma\Omega_2)}{(\Omega_1^2 + \Omega_2^2)[\Omega_1^2 + (\Omega_2 + \Gamma_s)^2]}, \quad (\text{S2})$$

where  $\omega_* = \sqrt{\Delta^2 + \Gamma^2}$ . The function  $A(k_F, \omega)$  is even and it exhibits two peaks at  $\omega \approx \pm\omega_*$ . Figure S1 shows that the pair-breaking rate  $\Gamma$  symmetrically broadens the peaks, while the forward-scattering rate  $\Gamma_s$  generates a finite asymmetry of the peaks, increasing their width predominantly for  $|\omega| > \omega_*$ . Note that the shape of  $A(k_F, \omega)$  is very sensitive even to small values of  $\Gamma$ . Therefore, although  $\Gamma$  turns out to be small if compared with the gap when fitting the experimental data (see Figs. 3, 4 from the main text), the values of  $\Gamma$  extracted from experiment are determined quite reliably.

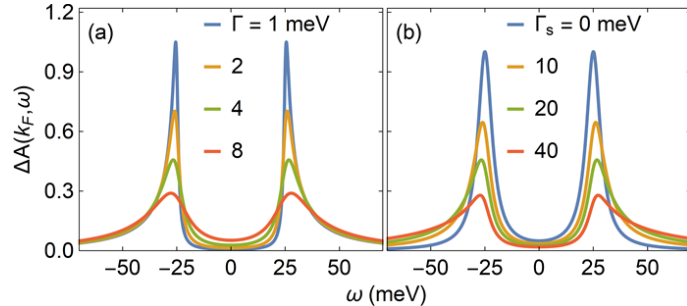


FIG. S1. Dependence of the Fermi-surface spectral function  $A(k_F, \omega)$  for  $\Delta = 25$  meV on the scattering rates. (a): Fixed  $\Gamma_s = 20$  meV. Increasing  $\Gamma$  symmetrically broadens the peaks. (b): Fixed  $\Gamma = 4$  meV. Increasing  $\Gamma_s$  generates asymmetric shape of the peaks, shifting weight from  $|\omega| < \omega_*$  to  $|\omega| > \omega_*$ .

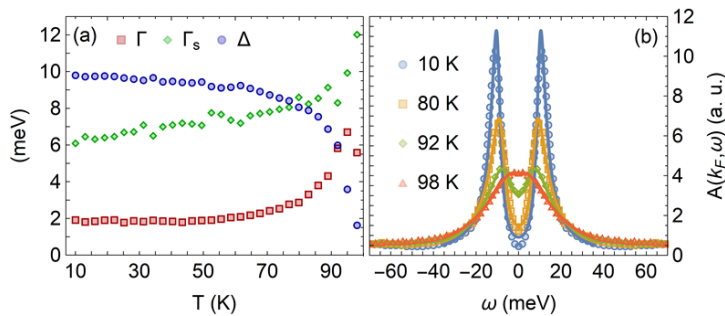


FIG. S2. (a):  $T$ -dependence of the MRPD parameters for spectral functions at  $k = k_F$  and  $\theta = 10^\circ$  in optimally doped Bi2212, taken from Ref. [S1]. (b): Spectral functions (symbols) and their MRPD fits (lines) for selected temperatures.

The MRPD parameters were obtained by fitting the experimental data for  $|\omega| < \Lambda$ , where  $\Lambda = 35$  meV. Larger values of  $|\omega|$  were not considered in the fits, because scattering can not be taken as elastic outside this energy range. The extracted scattering rates in Fig. 3 from the main text are roughly  $T$ -independent up to  $T \approx 50$  K. This suggests

that  $\Gamma_s$  and  $\Gamma$  should not depend on  $\omega$  roughly up to  $\pi T \approx 15$  meV, in an order-of-magnitude agreement with the chosen  $\Lambda$ . The background is taken as negligible in the fits. Thus, the fits depend on four parameters:  $\Delta$ ,  $\Gamma_s$ ,  $\Gamma$ , and the normalization factor. Figure S2 shows the results of a similar analysis of the same sample as in Fig. 3 from the main text, but at  $\theta = 10^\circ$ , i.e. closer to the node. Note the qualitative similarity between the results for both angles.

**Very large forward scattering  $\Gamma_s \gg \Gamma, \Delta$ .** In this limit,  $A(\mathbf{k}, \omega)$  for  $\omega \ll \Gamma_s$  and arbitrary  $\varepsilon_{\mathbf{k}}$  simplifies to

$$A(\mathbf{k}, \omega) = \delta_{\Gamma_s}(\varepsilon_{\mathbf{k}}) \times \text{Re} \frac{\omega + i\Gamma_{\mathbf{k}}}{\sqrt{(\omega + i\Gamma_{\mathbf{k}})^2 - \Delta_{\mathbf{k}}^2}}, \quad (\text{S3})$$

i.e., as a function of  $\omega$ , the spectral function is proportional to the Dynes formula. Since for  $\Gamma_{\mathbf{k}} \ll \Delta_{\mathbf{k}}$  the latter exhibits a sharp maximum at  $|\omega| \approx |\Delta_{\mathbf{k}}|$ , the second derivative  $A''(\mathbf{k}, \omega)$  with respect to  $\omega$  is strongly negative in the vicinity of  $|\omega| \approx |\Delta_{\mathbf{k}}|$  in this case, as indeed observed in Fig. 1f from the main text. Note also that according to Eq. (S3), surprisingly, the superconducting gap is observable even if  $\Gamma_s \gg \Delta$ , provided  $\Gamma \lesssim \Delta$ . This is relevant in the antinodal region, and explicitly demonstrated in Fig. S3.

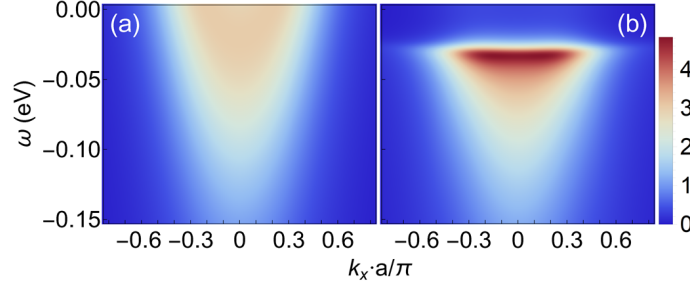


FIG. S3. Tomographic maps of  $A(k, \omega)$  predicted by MRDP along the antinodal cut  $\theta = 45^\circ$  for  $T$ -independent scattering rates  $\Gamma = 5$  meV and  $\Gamma_s = 100$  meV. (a): Normal state. (b): Superconducting state with  $\Delta_d = 30$  meV.

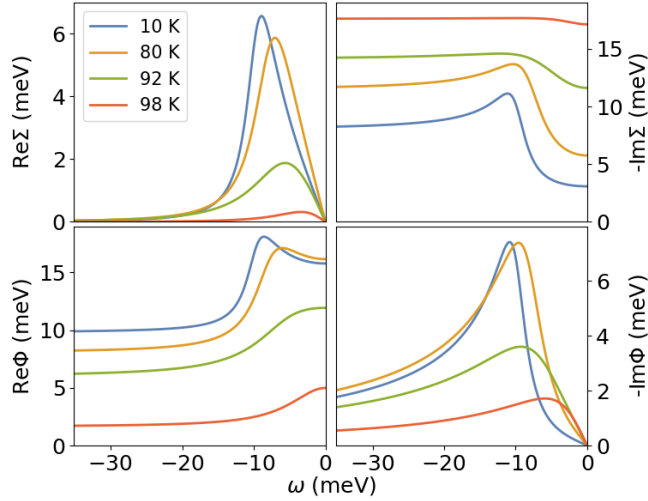


FIG. S4. Temperature dependence of the normal and anomalous self-energies  $\Sigma(\omega)$  and  $\Phi(\omega)$ , respectively, calculated using Eq. (S4) and the MRDP parameters from Fig. S2.

**MRDP prediction for the Eliashberg self-energies.** In case of Dynes superconductors, the self-energies defined in Eq. (5) from the main text are given by

$$\Sigma(\omega) = -i\Gamma - i\Gamma_s \frac{\omega + i\Gamma}{\Omega}, \quad \Phi(\omega) = \left(1 + \frac{i\Gamma_s}{\Omega}\right) \Delta. \quad (\text{S4})$$

Making use of the MRDP parameters from Fig. S2, we have calculated the  $T$ -dependence of the self-energies using Eq. (S4). The results are shown in Fig. S4. The qualitative agreement in the low-energy region with the findings of

Ref. [S2] is obvious: with decreasing  $T$ , the peak of  $\text{Re}\Sigma(\omega)$  grows at the gap position, while the contribution of  $\Gamma_s$  to  $-\text{Im}\Sigma(\omega)$  is strongly suppressed below the gap. Of course, the predictions of MRDP differ from the experimental results at large frequencies. In fact, within MRDP  $-\text{Im}\Sigma(\omega)$  saturates to  $\Gamma_s + \Gamma$  and  $\text{Re}\Sigma(\omega)$  vanishes, while the actual experimental result is that  $-\text{Im}\Sigma(\omega)$  grows with  $|\omega|$  and  $\text{Re}\Sigma(\omega)$  exhibits a finite background. Also the gap-related features of  $\Phi(\omega)$  in the low-energy region are seen to be qualitatively consistent with Ref. [S2].

**Joint density of states.** Additional support for the finite value of  $\Gamma_s$  in the MRDP spectral functions comes from the study of the joint density of states (JDOS)  $S(\mathbf{q}, \omega)$ , which is a convolution of spectral functions at fixed  $\omega$ :

$$S(\mathbf{q}, \omega) = \sum_{\mathbf{k}} A(\mathbf{k}, \omega) A(\mathbf{k} + \mathbf{q}, \omega). \quad (\text{S5})$$

The authors of Ref. [S3] find that the experimental JDOS exhibits the same pattern as predicted by the so-called octet model [S4] and therefore can be understood as a proxy for the quasiparticle interference spectra in the cuprates. Figure S5 shows that the momenta predicted by the octet model perfectly match the maxima of the theoretical JDOS, if we take a finite value of  $\Gamma_s$ . On the other hand, if we take  $\Gamma_s = 0$ , the calculated JDOS is qualitatively different from experimental data.

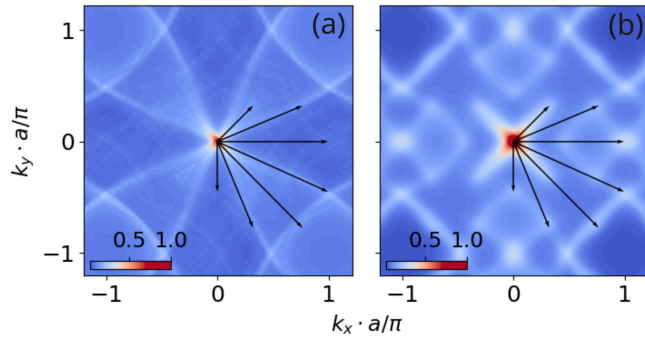


FIG. S5. Maps of the JDOS at  $\omega = -14$  meV predicted by MRDP for a model superconductor with momentum-independent scattering rates  $\Gamma$  and  $\Gamma_s$ . We take  $\Delta_d = 30$  meV. (a):  $\Gamma_s = 0$  and  $\Gamma = 10$  meV. (b):  $\Gamma_s = 40$  meV and  $\Gamma = 2$  meV. The arrows denote the octet-model momenta connecting the ends of the four bananas in the full Brillouin zone.

---

[S1] T. Kondo, W. Malaeb, Y. Ishida, T. Sasagawa, H. Sakamoto, T. Takeuchi, T. Tohyama, and S. Shin, *Nat. Commun.* **6**, 7699 (2015).

[S2] J.M. Bok, J.J. Bae, H.-Y. Choi, C.M. Varma, W. Zhang, J. He, Y. Zhang, L. Yu, and X.J. Zhou, *Sci. Adv.* **2**, e1501329 (2016).

[S3] N.K. Shah, J. Zhao, and U. Chatterjee, arXiv:2509.12568.

[S4] K. McElroy, R. W. Simmonds, J. E. Hoffmann, D.-H. Lee, J. Orenstein, H. Eisaki, S. Uchida, and J. C. Davis, *Nature* **422**, 592 (2003).